Author(s): Kravchenko, Aleksandr & Shevchenko, Andriy & Ovchinnikov, Victor & Grahn, Patrick & Kaivola, Matti

Title: Fabrication and characterization of a large-area metal nano-grid wave plate

Year: 2013

Version: Final published version

Please cite the original version:

Kravchenko, Aleksandr & Shevchenko, Andriy & Ovchinnikov, Victor & Grahn, Patrick & Kaivola, Matti. 2013. Fabrication and characterization of a large-area metal nano-grid wave plate. Applied Physics Letters. Volume 103, Issue 3. 033111. ISSN 1077-3118 (electronic). ISSN 0003-6951 (printed). DOI: 10.1063/1.4813756.

Fabrication and characterization of a large-area metal nano-grid wave plate

A. Kravchenko, A. Shevchenko, V. Ovchinnikov, P. Grahn, and M. Kaivola

Citation: Applied Physics Letters **103**, 033111 (2013); doi: 10.1063/1.4813756
View online: http://dx.doi.org/10.1063/1.4813756
View Table of Contents: http://scitation.aip.org/content/aip/journal/apl/103/3?ver=pdfcov
Published by the AIP Publishing

Fabrication and characterization of a large-area metal nano-grid wave plate

A. Kravchenko,[1,a)] A. Shevchenko,[1] V. Ovchinnikov,[2] P. Grahn,[1] and M. Kaivola[1]
[1]*Department of Applied Physics, Aalto University, P.O. Box 13500, FI-00076 Aalto, Finland*
[2]*Aalto Nanofab, Aalto University, P.O. Box 13500, FI-00076 Aalto, Finland*

(Received 3 June 2013; accepted 25 June 2013; published online 17 July 2013)

We introduce a fast and cost-effective technique to fabricate large-area periodically nanopatterned metal samples and apply this technique to create reflective nano-grid wave plates for optical wavelengths. The technique makes use of azo-polymer-based interference lithography and a special imprint method that enables creating large-area metal nanopatterns with high vertical walls. We fabricate and experimentally test a gold nano-grid wave plate that operates as reflective $\lambda/4$-plate for $\lambda = 604$ nm and $\lambda/2$-plate for $\lambda = 997$ nm. © *2013 AIP Publishing LLC*.
[http://dx.doi.org/10.1063/1.4813756]

Artificial nanostructures are nowadays widely used in many fields of science and technology. In optics, a large variety of nanofabricated optical elements, such as ultrathin polarizers[1] and wave retarders,[2,3] nanostructured antireflection coatings,[4] optical waveguides,[5] plasmonic nanoantennas and nanosensors,[6] substrates for surface enhanced Raman scattering,[7] and optical metamaterials,[8] have been developed and demonstrated to find numerous useful applications. As a specific class of nanofabricated optical elements, we mention periodic arrays of metal nanostructures, which can be designed to have a prescribed, strong, and spectrally highly selective optical response.[9,10] Such arrays are usually created with the help of electron-beam lithography (EBL),[11] which provide high fabrication precision, but are extremely time-consuming and as such not suitable for fabrication of large-area arrays of nanostructures. The same can also be said about focused ion beam lithography (FIB).[11,12] Furthermore, if the array is supposed to have long-range periodicity, the use of self-organized or self-assembled patterns[13,14] as initial etching masks or templates is not justified. As a matter of fact, the number of fast and cost-effective techniques for fabricating periodic nanostructures of a large surface area, such as nanoimprint lithography,[15] are rather limited, with the majority of these techniques involving optical interference lithography.[16]

Recently, we have proposed an optical lithography technique, in which conventional photoresists are replaced with azobenzene-functionalized polymers.[17,18] This replacement provides additional flexibility, reliability, and simplicity for the fabrication process. In this work, we apply this technique to create large-area periodically patterned dielectric templates which we then use as molds to obtain metal surface patterns with a complementary geometry. The metal is simply evaporated onto the template and then mechanically removed from it. A single template can be used to fabricate many nanopatterned metal samples. The technique is similar to the one used by Nagpal *et al.*,[19] but with a modification that allows us to obtain nanostructures with relatively high vertical walls. Using this technique, we fabricate a periodic array of nanogrooves in gold. The geometry of the array is chosen such that the sample acts as a reflective metal nano-grid wave plate. This optical element was proposed in Ref. 20, but has not yet been realized in practice.

The operation of the wave plate is based on the fact that the incident light polarized along the grooves (TM-polarized) is reflected mostly from the top surface of the array, while the orthogonally TE-polarized light penetrates into the grooves and will be reflected mostly from the bottom of the pattern. Thus, by properly selecting the depth of the grooves, one can obtain a quarter- or a half-wave plate, which provides a phase difference of $\pi/2$ and π, respectively, for the TE and TM polarizations. Such wave plates can be used, e.g., as mirrors in laser cavities that can help avoid optical standing waves and the resulting spatial hole burning effect in the gain medium.[21] The wave plate fabricated and tested in this work is designed to operate as a $\lambda/4$-plate at $\lambda \approx 600$ nm and as a $\lambda/2$-plate at $\lambda \approx 1000$ nm. The measured reflection and polarization spectra are shown to be in good agreement with theoretical predictions.

The fabrication process that we propose here for a cost-effective production of large-area nanopatterned metal samples is illustrated in Figure 1. In steps I and II, we fabricate a silicon template by applying an azo-polymer-based interference lithography described in detail in Ref. 18. In these steps, a silicon wafer is coated with thin films of alumina (Al_2O_3), titanium, gold, and an azo-polymer material [Poly(Disperse Red 1 acrylate)]. Then a surface relief grating is created on the azo-polymer film with a TM-polarized interference pattern produced in a Lloyd interferometer, at $\lambda = 488$ nm. Finally, the grating is used as a mask for etching the underlying layers and through them the silicon substrate. The resulting template is in the form of an array of deep rectangular grooves or dimples with vertical walls.[17,18]

In principle, owing to the poor adhesion of noble metals to oxides, one can oxidize the obtained template, coat it with gold or silver and apply the template-removal technique of Ref. 19 to obtain a metal surface with "nanoimprinted" pattern. However, when the template structures have vertical and relatively high walls, this approach fails because of a too large metal-template friction that appears upon the separation. The required stripping force can easily exceed the inelastic deformation threshold of the structures and even rapture the template. This is what we observed when we tried directly to use this approach. In order to decrease the metal-template friction,

[a)]aleksandr.kravchenko@aalto.fi

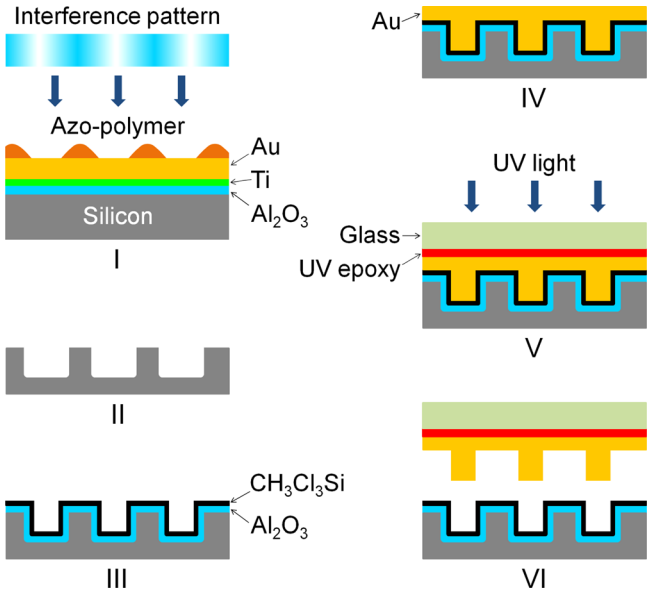

FIG. 1. Schematic diagram of the fabrication process. I—creation of an azo-polymer mask on a silicon wafer covered with Al_2O_3, Ti, and Au, II—etching of silicon and removal of other materials, III—ALD of Al_2O_3 and deposition of CH_3Cl_3Si, IV—deposition of Au, V—gluing of a glass plate to gold, and VI—removal of the gold pattern from silicon.

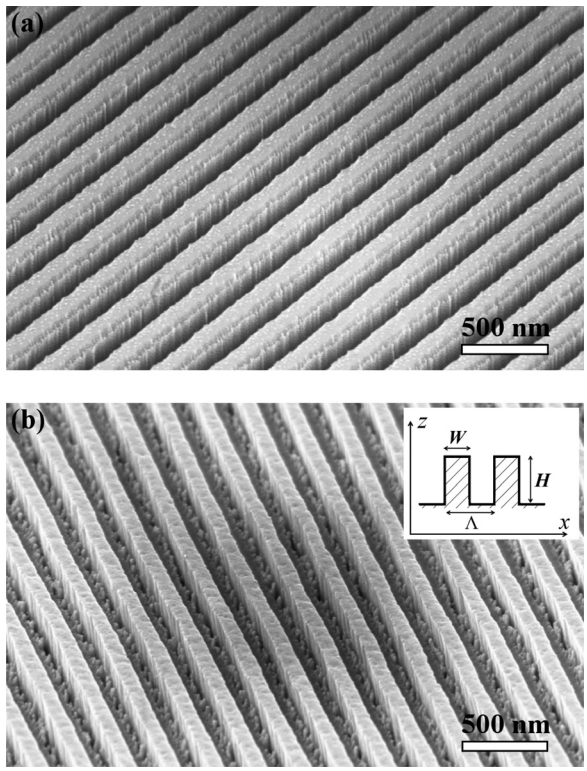

FIG. 2. SEM images of (a) a silicon template and (b) a gold nano-grid reflective wave plate created by using the template. The parameter values of the array are $\Lambda = 260$ nm, $W = 100$ nm, and $H = 210$ nm.

we coated the template with a thin layer of Al_2O_3 using atomic layer deposition (ALD) and on top of that a layer of trichloromethylsilane (CH_3Cl_3Si) using physical vapor deposition (see step III in Figure 1). The alumina deposition is also used as a tool for fine tuning the pattern dimensions, such as the groove width. Then, we evaporate gold onto the template (step IV) and glue a glass plate to the metal with UV-curable epoxy (step V). Finally, we easily decouple the metal glued to the glass from the template (the final step VI).

Figure 2 shows scanning electron microscope (SEM) images of (a) a silicon template fabricated in steps I and II in the form of nanogroove array and (b) a gold nano-grid wave plate created in steps III-VI with the help of this template. The structure dimensions are $\Lambda = 260$ nm, $W = 100$ nm, and $H = 210$ nm (see the inset of Figure 2(b)). The surface area of the array exceeds 1 cm^2. In principle, the sample area is limited only by the size of the laser spot in step I.

The optical properties of the fabricated wave plate were studied by using an experimental setup presented in Figure 3. Broadband light from a tungsten lamp is collimated with a lens, linearly polarized with a broadband polarizer and reflected from the wave plate at an angle $\theta \approx 9°$. This angle is small, such that the measured spectra are very close to those for normal incidence, as was verified by numerical calculations. The reflected light is analyzed with another broadband polarizer (analyzer) and a fiber-coupled spectrometer. The entrance end of the fiber is positioned in the middle of the light spot (that is about 1 cm in diameter).

Each measurement is started by replacing the wave plate with a high-quality thick gold film and measuring the transmission spectrum of the system with the polarizers aligned for maximum transmission. This spectrum is then used as a reference. Next, we insert the wave plate into the system and fix the transmission axis of the polarizer at an angle of 45° with respect to the sample's grooves. The analyzer is then rotated in steps of 5° over the full angle of 360° and the relative transmission spectra of the system are recorded for each step. The relative transmission is equal to the absolute transmission divided by the reference transmission. Thus, it describes the effect of the pattern on the reflection.

The recorded spectra contain all information necessary to evaluate the sample performance. A perfect quarter-wave plate would transform a linearly polarized incident light (see Figure 4(a) in which the incident electric field $\mathbf{E}_{in}$ is shown by the blue dash-dotted line) into a circularly polarized light without loss. The rotating electric field vector of the reflected light would thus trace a circle shown in Figure 4(a) by the red dashed line. A perfect half-wave plate, on the other hand, would switch the polarization state of the incident light to an orthogonal one and preserve the field amplitude (see the dashed green line that represents the corresponding oscillation of the reflected electric-field vector).

The system transmission curves plotted for several wavelengths as functions of the orientation angle α of the

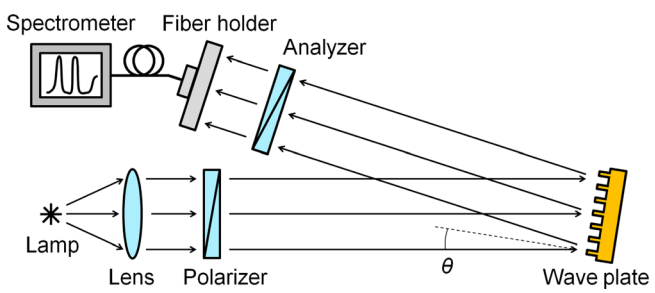

FIG. 3. Optical experimental setup.

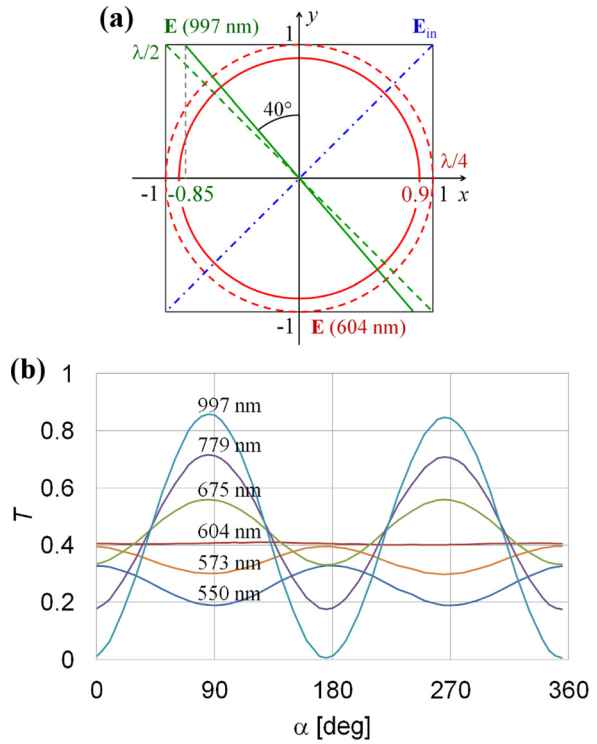

FIG. 4. (a) Polarization states of the waves reflected by the wave plate at the wavelengths of 604 nm (red lines) and 997 nm (green lines). The normalized incident electric field, E_{in}, is shown by the blue dashed-dotted line. Dashed and solid lines stand for the desired and experimentally obtained polarization ellipses, respectively. The y-axis is parallel to the grooves. (b) The measured relative transmission by the system as a function of the orientation angle α of the analyzer for several different wavelengths. The polarizer's transmission axis is oriented at 45° with respect to the grooves.

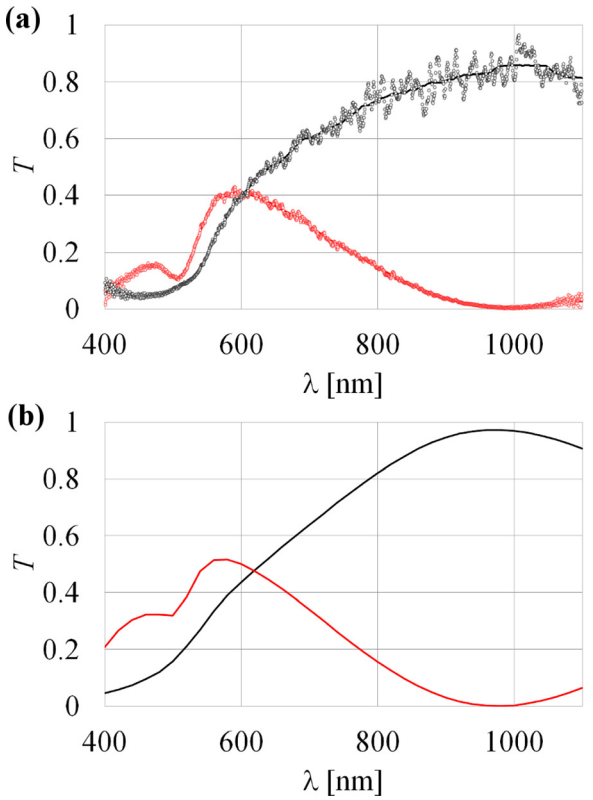

FIG. 5. (a) The measured relative transmission spectra of the system with the fabricated reflective wave plate at the analyzer orientation angles of $\alpha = -5°$ (red curve) and $\alpha = 85°$ (black curve). (b) The corresponding theoretical spectra calculated for an ideal wave plate at $\alpha = 0°$ (red curve) and $\alpha = 90°$ (black curve). The curves calculated for $\alpha = -5°$ and $\alpha = 85°$ (not shown) were nearly indistinguishable from the illustrated curves.

analyzer's transmission axis with respect to the axis of the polarizer are shown in Figure 4(b). It can be seen that at 604 nm, the transmission of the system does not depend on the orientation of the analyzer. Hence, the wave plate converts the incident light into circularly polarized light and thereby acts as a quarter-wave plate. The transmittance of the system at each orientation of the analyzer is smaller than 0.5 and indicates a 20% optical loss in the grooves at this wavelength. The solid red line in Figure 4(a) shows the polarization ellipse that corresponds to the measured reflected wave. The reflection coefficient for the field amplitude of the groove array is equal to 0.9.

At 997 nm, the transmission of the system is observed to reach zero at certain values of angle α of the analyzer. This means that the field reflected by the wave plate is linearly polarized. The maximum transmission takes place at a nearly crossed position of the polarizer and analyzer and, therefore, the sample operates as a quite good half-wave plate. The observed 5° deviation from the exact 90° position between the polarizer and analyzer and the measured 85% maximum transmission unambiguously imply that the reflection coefficient of the y- and x-components of the field have approximately the magnitudes of 1 and 0.85, respectively. These values can be calculated from equations $|E_x|/|E_y| = \tan(40°)$ and $|E_x|^2 + |E_y|^2 = 0.85|E_{in}|^2$. The x-component undergoes a higher loss, presumably because it penetrates into the groves where the metal surface is not quite smooth (see Figure 2(b)). The polarization state of the measured reflected light is shown in Figure 4(a) by the green solid line.

Figure 5(a) shows the measured intensity transmission spectra of the system at two rotation angles of the analyzer with respect to the polarizer, −5° (red) and 85° (black). The experimental data are represented by circles. The solid curves are obtained by locally averaging the experimental values. The relatively large scattering of the experimental values is a measurement artefact caused by mode interference in the fiber that guides the signal to the spectrometer; the coupling of the light to the fiber modes is sensitive to the incidence angle that slightly varies when the analyzer is rotated. The red and black curves in Figure 5(a) are seen to intersect at about 604 nm, and at this point the reflected light is circularly polarized. At 997 nm, the red curve shows a minimum and the black curve a maximum value, which corresponds to a half-wave plate operation of the array. In order to compare the fabricated wave plate with an ideal one, we numerically calculated the reflection spectra of an ideal component with the help of the commercial software COMSOL MULTIPHYSICS (version 4.3a). The ideal wave plate is assumed to have the same values of parameters Λ, W, and H as the fabricated one, but all its surfaces are assumed to be perfectly smooth. The spectral dependence of the electric permittivity of gold was taken from Ref. 22. Figure 5(b) shows the calculated curves obtained for the angles $\alpha = 0°$ (red curve) and $\alpha = 90°$ (black curve). It can be seen that the experimental spectra are very similar to the theoretically

predicted spectra. However, the measured sample shows a higher loss than the ideal one.

In conclusion, we have introduced a technique for creating large-area periodic metal nanopatterns that can have more than 200 nm high vertical walls. The fabrication process consists of (1) obtaining a nanopatterned dielectric template and (2) "printing" nanopatterned metal samples using this template. To fabricate the templates, we use azo-polymer-based interference lithography, and to create the corresponding metal prints, we apply an imprinting technique in which a layer of trichloromethylsilane is used to reduce friction between the template and the decoupling metal. Using this technique, we have fabricated an optical element that was previously theoretically proposed to operate as a reflective nano-grid wave plate. We could successfully verify this theoretical prediction. The fabricated wave plate operated as a quarter- and half-wave plate, at the wavelengths of 604 and 997 nm, respectively. It showed a slightly higher absorption loss than an ideal wave plate presumably due to nano-scale roughness of the metal surfaces in the grooves. In general, reflective nano-grid wave plates of the considered type can be designed to operate at longer or shorter wavelengths and fabricated of a different metal, such as silver or aluminum.

We thank the Academy of Finland (Project No. 134029) for financial support of this work. The samples were fabricated at Micronova Nanofabrication Centre of Aalto University.

[1]H. Tamada, T. Doumuki, T. Yamaguchi, and S. Matsumoto, Opt. Lett. **22**, 419 (1997).
[2]S. L. Wadsworth and G. D. Boreman, Opt. Express **19**, 10604 (2011).
[3]B. Päivänranta, N. Passilly, J. Pietarinen, P. Laakkonen, M. Kuittinen, and J. Tervo, Opt. Express **16**, 16334 (2008).
[4]H. K. Raut, V. A. Ganesh, A. S. Nairb, and S. Ramakrishna, Energy Environ. Sci. **4**, 3779 (2011).
[5]D. Dai, L. Liu, L. Wosinski, and S. He, Electron. Lett. **42**, 400 (2006).
[6]R. Adato, A. A. Yanik, J. J. Amsden, D. L. Kaplan, F. G. Omenetto, M. K. Hong, S. Erramilli, and H. Altug, Proc. Natl. Acad. Sci. U.S.A. **106**, 19227 (2009).
[7]C. Cheng, B. Yan, S. M. Wong, X. Li, W. Zhou, T. Yu, Z. Shen, H. Yu, and H. J. Fan, ACS Appl. Mater. Interfaces **2**, 1824 (2010).
[8]J. Valentine, S. Zhang, T. Zentgraf, E. Ulin-Avila, D. A. Genov, G. Bartal, and X. Zhang, Nature **455**, 376 (2008).
[9]S. Enoch, R. Quidant, and G. Badenes, Opt. Express **12**, 3422 (2004).
[10]T. Xu, Y.-K. Wu, X. Luo, and L. J. Guo, Nat. Commun. **1**, 59 (2010).
[11]Y. Xia, J. A. Rogers, K. E. Paul, and G. M. Whitesides, Chem. Rev. **99**, 1823 (1999).
[12]S. Matsui and Y. Ochiai, Nanotechnology **7**, 247 (1996).
[13]J. Y. Cheng, C. A. Ross, H. I. Smith, and E. L. Thomas, Adv. Mater. **18**, 2505 (2006).
[14]W. Lee, R. Ji, U. Gösele, and K. Nielsch, Nature Mater. **5**, 741 (2006).
[15]H. Schift, J. Vac. Sci. Technol. B **26**, 458 (2008).
[16]D. Xia, Z. Ku, S. C. Lee, and S. R. J. Brueck, Adv. Mater. **23**, 147 (2011).
[17]A. Kravchenko, A. Shevchenko, V. Ovchinnikov, A. Priimagi, and M. Kaivola, Adv. Mater. **23**, 4174 (2011).
[18]A. Kravchenko, A. Shevchenko, P. Grahn, V. Ovchinnikov, and M. Kaivola, Thin Solid Films **540**, 162 (2013).
[19]P. Nagpal, N. C. Lindquist, S.-H. Oh, and D. J. Norris, Science **325**, 594 (2009).
[20]Y. Pang and R. Gordon, Opt. Express **17**, 2871 (2009).
[21]O. Svelto, in *Principles of Lasers*, edited by D. C. Hanna (Springer, New York, 1998), pp. 282–284.
[22]P. B. Johnson and R. W. Christy, Phys. Rev. B **6**, 4370 (1972).